# HOW TO VALIDATE NUMERICAL RESULTS ON PRIMARY PARTICLE DIAMETER TO EXPERIMENTAL DATA FROM LAMINAR SOOTING FLAMES

**A. Bodor*, A. Cuoci*, B. Franzelli****
agneslivia.bodor@polimi.it
* Department of Chemistry, Materials, and Chemical Eng., Politecnico di Milano (Italy)
** Laboratoire EM2C CNRS, CentraleSupélec, Université Paris-Saclay, Chatenay-Malabry (France)

**Abstract**
Combustion generated soot particles have harmful effects on human health and our environment. An important aspect is to accurately determine the surface area of the particle population, which can be estimated from the particle size distribution (PSD) and morphology. Experimental investigations showed that large particles are aggregates constituted of several small primary particles [1]. Therefore, the determination of the primary particle size distribution (PPSD) is essential for the characterization of soot population.
On the one side, sectional methods can be used to numerically predict the particle population of sooting flames. However, most of models assumes that large particles are spherical for all sections [2] or aggregates constituted of primary particles of identical size for all sections [3-5]. These strong assumptions can affect the results' quality and the validity of the models themselves. On the other side, Time Resolved Laser Induced Incandescence (TiRe-LII) is a powerful, non-intrusive experimental method, which exploits the fact that the temporal decay of the LII signal is related to the primary particle diameter $d_p$. Information on the PPSD can then be derived once the PPSD shape is presumed [6]. The general approach is to assume log-normal distribution, but Transmission Electron Microscopy measurements showed that this assumption may be not always valid [7].
In this context, the comparison of numerical results on the PPSD with experiments is extremely complex due to the strong assumptions underlying the numerical models and the fact that TiRE-LII technique does not measure directly the PPSD. In this work, we propose a new way to compare numerical to experimental data on PPSD. First, we improved our existing CFD code to obtain the mean size of the primary particles for each section, based on what proposed in [4]. Second, the TiRe-LII signal is reconstructed from the numerical PPSD and compared directly to the measured signal [8] to avoid any potential errors due to a presumed PPSD shape. This approach is applied to the investigation of an ethylene laminar-coflow

diffusion flame [9], which is a target of the ISF workshop [10], and potential sources of errors are discussed.

**Improving the sectional model: the primary particle transport equation**

The discrete sectional approach of Saggese et al. [3] is considered here. Gas phase is described with 197 gaseous species. The solid phase is described by 20 mass sections (BIN) with 3 H/C subsections for small particles (from $BIN_5$ to $BIN_{12}$) and 2 H/C subsections for big particles (from $BIN_{13}$ to $BIN_{20}$). In the original model, small particles are considered by construction as spherical, whereas big particles are supposed to be aggregates whose primary particles size is identical for all sections and equal to the last spherical particle (~10 nm diameter) [3, 11]. In the improved approach, called transport equation (TE) model in the following, the particle morphology is not prescribed *a priori* for a given BIN, but it is obtained from the transport equation for the primary particle number of each section [14]:

$$\frac{\partial}{\partial t}(\rho\rho_{PBi}) + \nabla(\rho\rho_{PBi}\boldsymbol{v}) = -\nabla(\rho\rho_{PBi}\boldsymbol{V_i}) + \sum_r \Omega_{r,i}(Y_0, \dots, Y_{12}, \rho_{PB0}, \dots, \rho_{PB12}) \qquad (1)$$

where $\rho$ is the density, $\rho_{PBi}$ is the primary particle density of $BIN_i$ type, $\boldsymbol{v}$ is the velocity, $\boldsymbol{V_i}$ is the diffusion velocity of $BIN_i$ [12] and $\Omega_{r,i}$ is the $BIN_i$ type primary particle source term of reaction $r$, $Y_i$ is the species mass fraction of $BIN_j$. Fick's diffusion was neglected as previous studies showed that only thermal diffusion plays a significant role for soot particles. It should be noticed that in the TE model, the biggest possible $d_p$ value is 64 nm, i.e. the diameter of a spherical particle belonging to $BIN_{20}$.

The effect of particle collision on $d_p$ is described in the TE approach by the model of Lahaye et al. [13]. Small particles coalescence and form spherical particles, whereas a pure aggregation occurs between big particles. The collision of a small with a big particle leads to the coalescence of the first one on the second one. In practice, primary particle growth of big particles occurs only through surface growth processes (additional mass is uniformly distributed among the primary particles) or coalescence with small spherical particles. For a general reaction:

$$\sum_{i=12}^{20} \nu_i BIN_i + \sum_{s=1}^{N_s} \nu_s X_s => \sum_{i=12}^{20} \mu_i BIN_i + \sum_{s=1}^{N_s} \mu_s X_s \qquad (2)$$

the source term for primary particles based on the above considerations will be:

$$\Omega_{r,i} = \left( \frac{\mu_i M_i}{\sum_{k=12}^{20} \mu_k M_k} \sum_{k=12}^{20} \frac{\nu_k M_k \rho_{PBk}}{Y_k} - \frac{\nu_i M_i \rho_{PBi}}{Y_i} \right) \cdot R_r \qquad (3)$$

where $\nu_i$ is the stoichiometric coefficient for reaction $r$, $X_s$ are the non-aggregate species $s$, $N_s$ is the number of non-aggregate species, $M_i$ is the molecular mass of $BIN_i$ and $R_r$ is the reaction rate of reaction $r$. It should be noticed that, at this stage, the TE model is used as a post-processing reconstruction method to obtain the mean primary particles size for each BIN and, consequently, the PPSD.

**LII signal reconstruction method**

The LII signals reconstruction is based on the relations derived by Hofman et al. [14], where the contribution by a particle with $d_p$ diameter to LII signal is given by:

$$S_{LII} = 2\pi^2 hc^2 d_p^2 \int_{\lambda_1}^{\lambda_2} \frac{\Omega(\lambda)\varepsilon(\lambda)}{\lambda^5[exp(hc/\lambda k_B T_p)-1]} d\lambda \quad (4)$$

where $h$ is the Planck constant, $\Omega$ the spectral response function of the detection system, and $\varepsilon$ the spectral emissivity of soot. The integral boundaries $\lambda_1$ and $\lambda_2$ are defined by the detection bandpass. Experimental related parameters were chosen based on reference measurements [8]. The particle temperature can be derived from the energy balance, whereas the particle mass based on the mass loss due to vaporization. The detailed expression of the energy terms can be found in [14].
The total LII signal is reconstructed by summing the LII contribution of each single primary particle for each section, calculated from the gaseous and solid fields obtained in our numerical simulation. Therefore, the aggregate shielding effect is here neglected.

**Numerical setup**

The numerical simulation reproduces the flame investigated with LII at EM2C [8] on the burned designed at Yale [9]. The flame is fed by an 80% ethylene - 20% nitrogen mixture, which is injected through an inner tube of diameter of 3.9 mm with 0.38 mm wall thickness. An air co-flow is injected through an external tube of 50 mm diameter. The bulk velocity of both inner and outer streams was set to 35 cm/s with parabolic and uniform velocity profiles, respectively. Temperature is set to the ambient value of 293 K and atmospheric pressure was prescribed.The simulation solves the usual conservation equations for mass, momentum, energy, and species with the laminarSMOKE framework [12], which has been extended with the TE post-processing tool to solve the primary particle number transport equation. The simulation was performed with an axisymmetric assumption on a 2D structured mesh, refined in the flame area. A second-order, centered spatial discretization scheme was adopted. The transport equations of species are solved through the operator-splitting approach.
$BIN_5$ to $BIN_7$ will not be considered in the reconstruction of soot volume fraction $f_v$, $d_p$ and LII signals, since the smallest particles may be not captured by the experimental LII measurements due to sublimation effects [15].

**Comparison of numerical and experimental results**

Numerical results for the soot volume fraction are compared to experiments [8] in Figure 1a. The calculated and experimentally measured $f_v$ are qualitatively similar, since higher values were detected in the wings of the flame. However, it should be noticed that results have been normalized by their maximum (1.2 ppm and 4.8 ppm for numerical and experimental results) and that the predicted soot region is shorter that the experimental one.

On Figure 1b the mean $d_p$ derived from the experimental LII signal with a lognormal PPSD assumption [8] is compared to the numerical solutions. Three models are here considered: the original model, the TE approach, and a further post-processing approach where all particles are consider as spherical (SP). As expected, the original, TE and SP models predict the smallest, the intermediate and the biggest values of $d_p$, respectively. In particular, with the spherical assumption $d_p$ reaches higher values than the other two models, especially in the post flame region where oxidation quickly removes small particles. The original model provides an almost constant $d_p$ value everywhere. The TE and SP models greatly improve the qualitative agreement with the experiments: larger $d_p$ values are observed on the wings. However, $d_p$ values in the wings are still largely underestimated by simulations. This may have many causes: the underestimation of $f_v$ can possibly affect the $d_p$ prediction; the maximum predictable $d_p$ value is smaller than the highest experimentally observed value; the experimental $d_p$ value may be affected by the post-processing procedure.

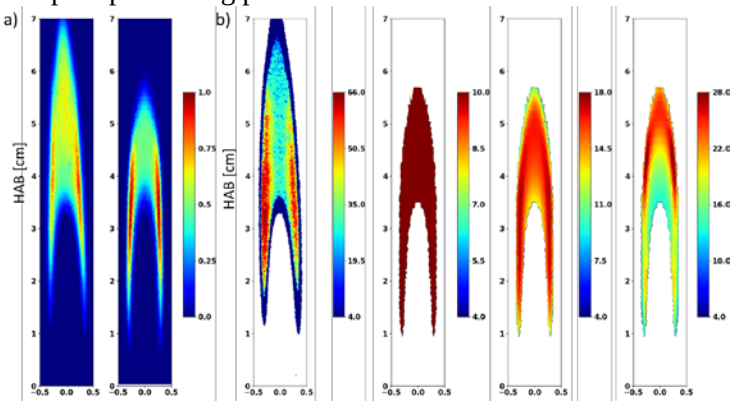


**Figure 1.** a) Experimental (left) and numerical (right) normalized soot volume fraction; b) Experimental (left), numerical (TE) (center) and numerical (Sp) (right) mean $d_p$ [nm].

To clarify this last point, the experimentally captured and the numerically reconstructed LII signals at 6 different times are shown on Figure 2 normalized by the signal at 0 ns. The numerical LII signals have much faster decay until 50 ns, almost one order of magnitude faster decays are reached within this time compared to the experiment. This seems to indicate that the discrepancies on $d_p$ are most probably due to the underprediction of large primary particle presence and/or an underestimation of their diameter size in the numerical simulations. In addition, a lower spatial inhomogeneity of $d_p$ is observed in the simulations compared to experiments. The TE model predicts slower signal decay than the original model due to the presence of larger primary particles and less spatial uniformity due to the varying PPSD for big particles, which is in better agreement with the experimental observations. The better agreement of results from the SP model with experiments indicate that the presence of even larger particles would be required. The direct comparison on LII signals allows concluding that the discrepancies among

experiments and simulations observed in this case are not due to the use of a presumed PPSD shape for the TiRe-LII signal post-processing, but to some accuracy limits of the numerical model.

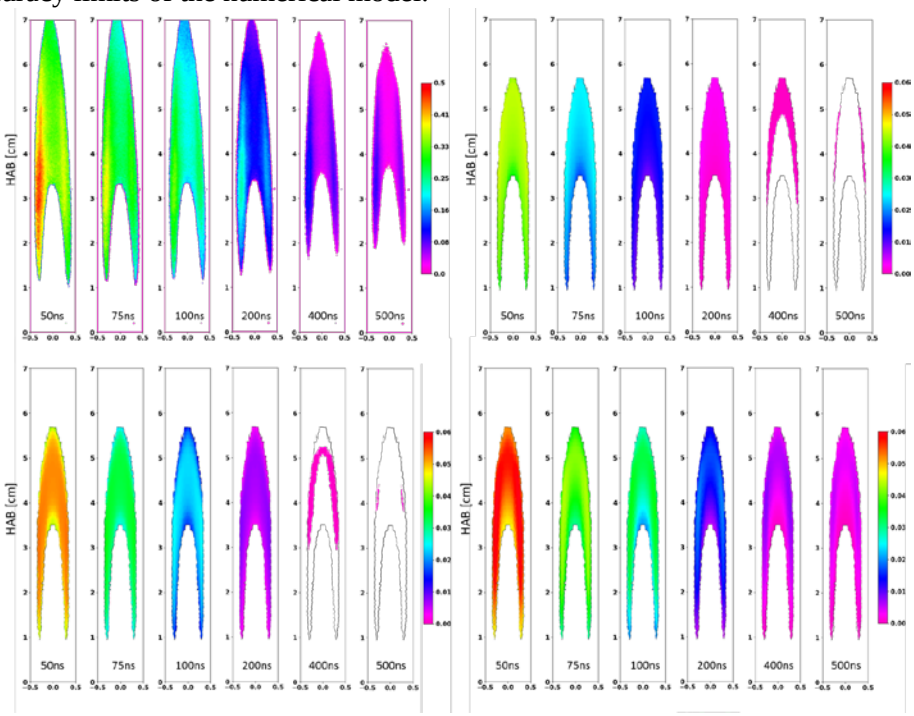


**Figure 2.** LII signal at six different delay times. Experiment data (top left) are compared to numerical calculations with the original model (top right), with the TE model (bottom left) and the SP approach (bottom right).

## Conclusions

A new validation approach of numerically calculated primary particle size distribution with TiRe-LII experiments was presented and applied on an ethylene co-flow laminar flame. The numerical simulation used the sectional soot model with detailed gas and solid phase chemistry. The model was improved by introducing an additional transport equation for the primary particle density in each section. Results on $d_p$ were qualitatively improved by the new model. LII decay signals were calculated based on numerical results from the original model, the improved one, and by assuming sphericity for all soot particles. Simulations were compared to the experimental LII signal. The simulated signals showed a much faster decay in the first 50 ns than the experiments and lower inhomogeneity in space. This implies that the predicted contribution of large particles to the particle population is not high enough relatively to the small ones and/or that the predicted largest particles are not big enough. The proposed approach to compare numerical and experimental data on PPSD seems a promising procedure for a pertinent validation of numerical data.

**Acknowledgements**
This project has received funding from the European Union's Horizon 2020 research and innovation programme under the Marie Sklodowska-Curie Grant Agreement No 643134.

**References**

[1] Sorensen, C.M., Feke, G.D., "The Morphology of Macroscopic Soot" *Aerosol Sci. Technol.* 25: 328–337 (1996)
[2] Blacha, T., Di Domenico, M., Gerlinger, P., Aigner, M.m "Soot predictions in premixed and non-premixed laminar flames using a sectional approach for PAHs and soot" *Combust. Flame* 159: 181–193 (2012)
[3] Saggese, C., et al. "Kinetic modeling of particle size distribution of soot in a premixed burner-stabilized stagnation ethylene flame" *Combust. Flame* 162: 3356–3369 (2015)
[4] Veshkini, A., "Understanding Soot Particle Growth Chemistry and Particle Sizing Using a Novel Soot Growth and Formation Model", PhD Thesis University of Toronto (2015)
[5] Rodrigues, P., Franzelli, B., Vicquelin, R., Gicquel, O., Darabiha, N., "Unsteady dynamics of PAH and soot particles in laminar counterflow diffusion flames" *Proc. Combust. Inst*. 36: 927–934 (2017)
[6] Daun, K.J., Stagg, B. J., Liu, F., Smallwood, G.J., Snelling, D.R. "Determining aerosol particle size distributions using time-resolved laser-induced incandescence" *Appl. Phys. B Lasers Opt.* 87: 363–372 (2007)
[7] Kempema, N.J., Long, M.B., "Combined optical and TEM investigations for a detailed characterization of soot aggregate properties in a laminar coflow diffusion flame" *Combust. Flame* 164: 373–385 (2016)
[8] Franzelli, B., et al. "Multi-diagnostic soot measurements in a laminar diffusion flame to assess the ISF database consistency" *Proc. Combust. Inst.*, submitted (2018)
[9] Smooke, M.D., et al. "Investigation of the transition from lightly sooting towards heavily sooting co-flow ethylene diffusion flames" *Combust. Theory Model.* 8: 593–606 (2004)
[10] http://www.adelaide.edu.au/cet/isfworkshop/, updated in 2016
[11] Saggese, C., "Detailed Kinetic Modeling of Soot Formation in Combustion Processes" PhD Thesis, Politecnico di Milano (2014)
[12] Cuoci, A., Frassoldati, A., Faravelli, T., Ranzi, E., "Numerical modeling of laminar flames with detailed kinetics based on the operator-splitting method" *Energy and Fuels* 27: 7730–7753 (2013)
[13] Lahaye, J., "Particulate carbon from gas phase" Carbon, 30: 309–314 (1992)
[14] Hofmann, M., Kock, B., Schulz, C., http://web.liisim.com/, updated in 2007
[15] Cenker, E., Bruneaux, G., Dreier, T., Schulz, C., "Determination of small soot particles in the presence of large ones from time-resolved laser-induced incandescence" *Appl. Phys. B Lasers Opt.* 118: 169–183 (2015)